Original Research

Revista Brasileira de Física Médica (2026) 20:872

Additive Manufacturing of Personalized Lung Shields for TBI: A New Methodology Using Lead Attenuation

Luísa V. Cassol[1], Thiago S. Fontana[2], Tadeu Baumhardt[3], Stefanie C. Schwarz[1], Thiago V. Claus[1,3]

[1]Programa de Graduação de Física Médica da Universidade Franciscana, Santa Maria, Brasil
[2]Serviço de Radioterapia São Sebastião, Florianópolis, Brasil
[3]Serviço de Radioterapia do Hospital Universitário de Santa Maria, Santa Maria, Brasil

Abstract

This study aimed to develop and physically validate patient-specific lung shielding devices for Total Body Irradiation (TBI) using additive manufacturing (3D printing) and granular lead spheres as the attenuating material. Radiographs of a semi-anthropomorphic phantom were used for three-dimensional modeling of the lung region and fabrication of customized molds. The printed structures were filled with lead spheres equivalent to approximately 0.8 cm thickness and positioned on the phantom to verify geometric adaptation. Dosimetric characterization was performed using a 6 MV linear accelerator beam and solid water phantoms at depths of 5, 10, and 15 cm, representing different equivalent body thicknesses. Ionization readings (nC) were converted to absorbed dose to water (cGy), allowing assessment of attenuation and volumetric uniformity of the device in a homogeneous medium. Mean attenuation ranged from 24.77% to 26.60%, with variation below 2% across depths and a similar response between right and left shields, indicating a homogeneous distribution of the attenuating material and the reproducibility of the manufacturing process. The obtained values are consistent with lung shielding reported in the literature. The results demonstrate that the device provides effective physical attenuation, internal uniformity, and feasible fabrication via additive manufacturing, representing a technically suitable alternative for personalized lung shielding in TBI. Further studies using heterogeneous anthropomorphic phantoms are recommended to validate performance under realistic pulmonary anatomical conditions.

Keywords: Radiotherapy; Radiation Protection; Innovation; Dose Attenuation.

1. Introduction

Total Body Irradiation (TBI) is a radiotherapy technique widely employed in conditioning regimens for hematopoietic stem cell transplantation, in which lung shielding constitutes a critical step to reduce toxicity without compromising overall dose homogeneity (1,2). Treatment is typically delivered using linear accelerators (LINACs), the primary radiation source in external beam radiotherapy, employing large fields and extended source-to-surface distances to ensure uniform whole-body coverage (3,4). In this context, lung shields must present reproducible geometry and predictable attenuation performance.

Despite the well-recognized clinical importance of lung protection during TBI, there is no consensus on the optimal method for its implementation, and variations in clinical practice may affect both treatment efficacy and patient safety (1,4). Among the most commonly used materials is Cerrobend alloy, traditionally composed of bismuth (50%), lead (26.70%), tin (13.30%), and cadmium (10%). However, its application presents limitations, including cost, potential inhomogeneity, and particularly the toxicological risks associated with cadmium (5). Cadmium is recognized as a human carcinogen, with pulmonary and renal effects related to fume inhalation during melting and chronic exposure to dust; therefore, casting and finishing require local exhaust ventilation, personal protective equipment, and environmental control (6). Cadmium-free low-melting-point alloys (e.g., indium/tin substitutions) exist, but their limited availability in the national market and higher cost restrict routine use. The strategy proposed in this work, 3D-printed molds filled with granular lead, avoids metal melting and thus mitigates exposure to metal fumes while maintaining attenuation effectiveness. In this scenario, the development of new techniques and materials for external radiotherapy shielding aims to enhance patient protection in a safe and personalized manner (7).

Three-dimensional (3D) printing, or additive manufacturing, enables the production of patient-specific anatomical devices. Since the validation of early three-dimensional digital phantoms, such as those developed by Mankovich et al. (8), which demonstrated the accuracy of anatomy-based models derived from medical imaging data, additive manufacturing has been applied to the creation of customized radiotherapy accessories and simulators, optimizing treatment planning and quality assurance (9).

Given the lack of standardization in lung shielding practices and the limitations of the conventional materials currently used, the present study aimed to develop personalized lung shields using additive manufacturing, creating patient-specific anatomical models fabricated from high-density materials with proven radiation attenuation and adaptable to individual anatomy. This strategy seeks not only to minimize radiation-induced pulmonary effects but also to optimize the safety and effectiveness of radiotherapy in patients undergoing TBI.

2. Material and methods

Initially, experiments were conducted using the X-ray equipment available in the Radiodiagnosis Laboratory of the Medical Physics and Radiology undergraduate program at Universidade Franciscana (UFN). In a second stage, the analyses were complemented using the linear accelerator installed at the Santa Maria Radiotherapy Service.

Table 1 presents the complete list of materials and equipment used in this study.

Table 1. Equipment and materials used in the study.

System / Equipment	Manufacturer	Model
Radiographic system	Intecal	MAAF
Computed radiography (CR)	Carestream	Vita Flex
Imaging plate (IP) (35X43)	Carestream	-
Phantom (simulator object)	-	-
3D printer	Anycubic	Kobra 2 Pro
PLA filament	Voolt 3D	-
Lead spheres	-	-
Precision balance	Marte	AY220
Micrometer	Mitutoyo	293-821-30
Vernier caliper	Vonder	-
Millimeter graph paper	-	-
Linear accelerator	Elekta	Synergy Platform
Dosimetry system	PTW	UNIDOS®
Solid water phantoms	-	-

Source: The author (2026).

2.1. Modeling and fabrication of the lung shield

Radiographic imaging of the semi-anthropomorphic phantom (10) was performed in the UFN radiodiagnosis laboratory using the positioning adopted during the TBI procedure, with a source-to-surface distance (SSD) of 275 cm, as illustrated in Figure 1(A).

From the acquired images, segmentation and digital modeling of the lung structures were performed. These models were subsequently used in computer-aided design (CAD) to create negative molds for 3D printing the lung shields on the free online platform Tinkercad (Figure 1(B)). Radiographic verification before and after each application was adopted to ensure accurate positioning of the lung shields during TBI and to integrate digital modeling with radiographic validation, contributing to procedural safety and quality (2).

To determine the true dimensions of the lung shields for the phantom, a reference scaling plate was used to correct for radiographic magnification caused by the distance between the phantom and the imaging plate. A flat plate containing lead spheres spaced at 1 cm intervals in a cross pattern (Appendix I) was positioned 45 cm from the phantom, corresponding to the expected shield location during treatment (Figure 1(C)). From this analysis, corrected lung dimensions were obtained: approximately 20 cm × 9 cm for the right lung and 19 cm × 9 cm for the left lung.

The lead thickness required for lung shielding in a TBI treatment with a prescribed dose of 12 Gy using a 6 MV photon beam was calculated assuming that the lung dose should be limited to 8 Gy (2). Thus, the lead density was experimentally determined, and the required material thickness was estimated to attenuate the incident radiation by one-third.

Lead density was determined experimentally by weighing nine lead spheres with a precision balance and calculating the mean. Sphere volume was obtained from mean diameters measured with a micrometer. The calculated density was $\rho = 11.42 \frac{g}{cm^3}$, with a 0.98% deviation from the tabulated value of $\rho = 11.31 \frac{g}{cm^3}$ (11).

Lead thickness was estimated using the exponential attenuation equation (Eq. 1):

$$I(x) = I_0 . e^{-\left(\frac{\mu}{\rho}\right).\rho.x}, \quad (1)$$

where $I(x)$ is the transmitted intensity, I_0 the incident intensity, μ the linear attenuation coefficient, $\frac{\mu}{\rho}$ the mass attenuation coefficient, and x the material thickness.

Considering the desired attenuation ratio $\frac{I(x)}{I_0} = \frac{8\,Gy}{12\,Gy} \approx 0.6667$, a mass attenuation coefficient for lead at 6 MV of $4.391 \times 10^{-2} \frac{cm^2}{g}$ (12), and the experimentally determined density of $\rho = 11.42 \frac{g}{cm^3}$, the logarithmic

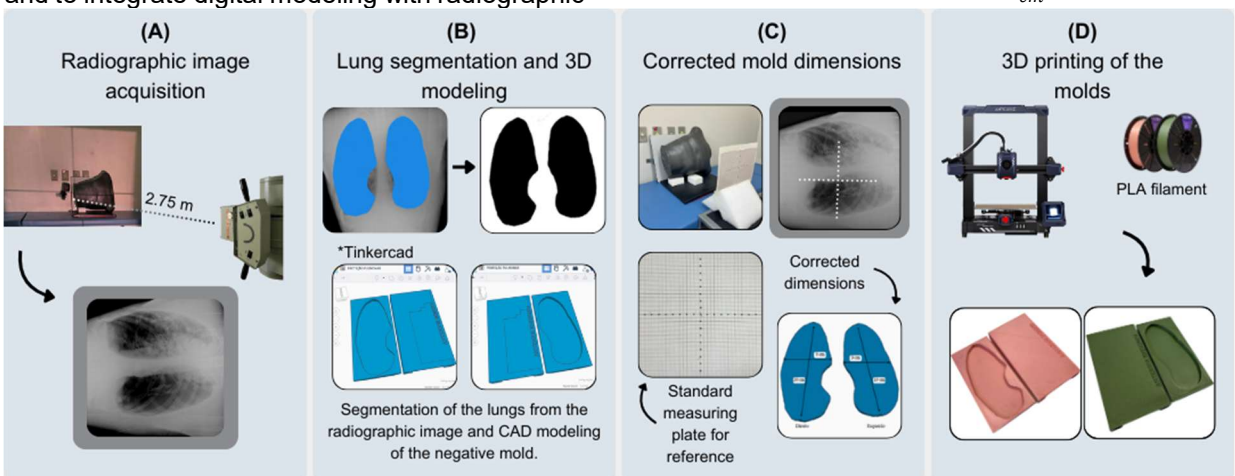

Figure 1. Shield modeling and fabrication. (A) Radiographic image acquisition; (B) Lung segmentation and 3D modeling; (C) Mold proportion correction; (D) 3D printing of molds. Source: The author.

form (Eq. 2) was applied:

$$ln\left(\frac{I(x)}{I_0}\right) = -\left(\frac{\mu}{\rho}\right).\rho.x. \quad (2)$$

The resulting lead thickness required to attenuate approximately one-third of the incident radiation was 0.808 cm.

The molds were then fabricated using a 3D printer with PLA filament (Figure 1(D)).

After printing, the internal cavities were manually filled with lead spheres until the volume was fully occupied (Figure 2).

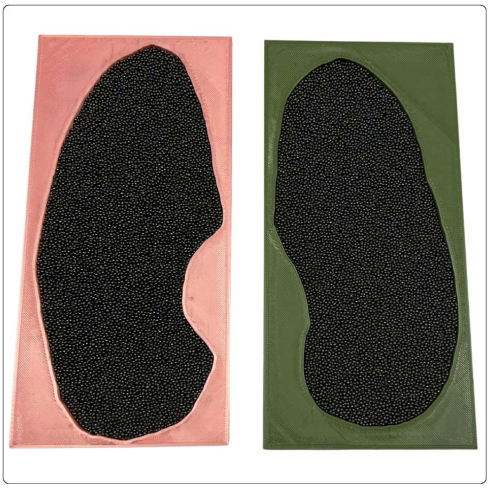

Figure 2. Filling of the lung shields with lead spheres. Source: The author.

Radiographic acquisition in the experimental configuration was performed to verify geometric adaptation and relative positioning of the shields with respect to the phantom, using the same geometric parameters as in the dosimetric measurements.

2.2 Dosimetry

For dosimetric evaluation, the irradiation geometry was defined according to the TBI technique.

Environmental conditions during irradiation (pressure 1003.6 hPa, temperature 20.8 °C, and humidity 47%) were recorded to ensure reproducibility and data consistency. The photon beam energy was set to 6 MV, with a 40 cm × 40 cm field size and a source-to-surface distance of 275 cm, to ensure broad target coverage. The gantry and collimator were positioned at 85° and 45°, respectively. A total of 200 monitor units (MU) per measurement were delivered at a dose rate of 600 MU/min for absolute dose assessment. Although clinical TBI is typically delivered at low dose rates (5-10 cGy/min) (13), higher dose rates were used in this study for controlled experimental dose assessment.

For measurements, 5-cm-thick solid-water phantoms were positioned at 2.75 m from the linear accelerator source. The ionization chamber was inserted into its dedicated cavity (Figure 3(A)), allowing accurate dose detection in the configured beam.

The lung shields were inserted individually at a distance of 45 cm from the solid-water phantoms. In the first configuration, a single 5 cm slab was used; in the second, two slabs totaling 10 cm; and in the third, three slabs totaling 15 cm thickness (Figure 3(B)). These thicknesses represent different equivalent body habitus conditions: 5 cm, 10 cm, and 15 cm corresponding to pediatric, adolescent, and adult patients, respectively.

2.3 Filling Homogeneity and Reproducibility Assurance

To ensure filling homogeneity and minimize apparent density variations, lead spheres from a single batch were used. Granulometric characterization yielded individual diameters of 1.913 mm, 1.522 mm, 1.400 mm, 1.683 mm, 1.634 mm, 1.650 mm, 1.645 mm, and 1.120 mm, corresponding to a mean of approximately 1.6 mm. Mold filling was performed in successive layers combined with controlled vibration (~50-60 Hz for ~2 min) to promote uniform sphere packing. Method reproducibility was assessed through gravimetric verification of the shield, with a maximum allowed variation of 0.50% between reassemblies. Apparent density was calculated as $\rho_{app} = \frac{m_{Pb}}{V_{internal}}$ and compared with the expected value for random dense packing (f_{pack}≈ 0.64).

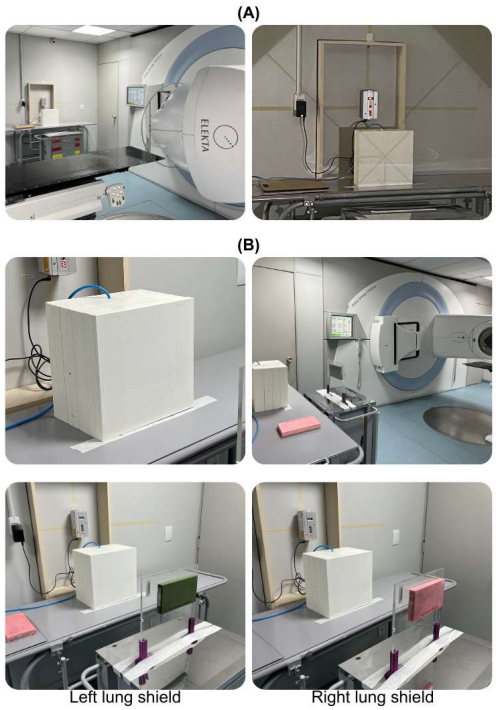

Figure 3. Experimental setup. (A) Initial assembly with ionization chamber; (B) Lung shields with solid-water phantoms. Source: The author.

3. Results and Discussions

It should be noted that the measurements were performed in a water-equivalent medium, which does not reproduce the low radiological density of lung tissue, which is characterized by air and structural heterogeneity. Therefore, the results obtained should be interpreted as a physical characterization of the device's attenuation properties in a homogeneous medium, rather than as a direct estimate of clinical

lung dose in total body irradiation. Nevertheless, the experimental model allows validation of the device performance in terms of attenuation and geometric reproducibility under controlled conditions.

The radiograph of the experimental configuration (Figure 4) provides visual evidence of the efficiency and uniformity of the developed device. The image demonstrates adequate adaptation of the lung shields to the phantom, with correspondence between the designed geometry and the simulated thoracic anatomy, and consistent shield positioning. A homogeneous radiographic appearance of the attenuating material within the printed structures is also observed, without individual visualization of the lead spheres, indicating uniform filling and absence of significant voids within the shield volume.

Figure 4. Radiograph of the experimental setup with the lung shields positioned in front of the phantom. Source: The author.

Ionization charge measurements were performed in triplicate for the three evaluated configurations (no shield, right shield, and left shield) at depths of 5 cm, 10 cm, and 15 cm in solid water phantoms. The mean values were used for dose calculation. High measurement reproducibility was observed, with experimental standard deviations below 0.20%, indicating stability of the experimental setup and consistent positioning of the ionization chamber.

Initially, the readings obtained in nanoCoulomb (nC) were converted to absorbed dose in water, expressed in centigray (cGy). Temperature and pressure corrections ($k_{T,P}$ - Equation 3) were applied, and Equation 4 was used (17):

$$k_{T,P} = \frac{273.15+T}{273.15+20} \times \frac{1013.25}{P} \quad (3)$$

$$D_{w,Q} = M_Q \times N_{D,w,Q_0} \times k_{Q,Q_0} \times 100 \times k_{T,P} \times k_{pl} \quad (4)$$

where $D_{w,Q}$ is the absorbed dose to water at the reference depth (cGy), M_Q is the dosimeter reading (nC), N_{D,w,Q_0} is the ionization chamber calibration factor (30.757 cGy/nC), k_{Q,Q_0} is the beam quality correction factor for 6 MV and a 40 × 40 cm² field (0.9869), and k_{pl} is the correction factor for the solid phantom material relative to liquid water, assumed to be 1.00 since the material is certified as water-equivalent.

The obtained dose values, as well as the corresponding dose rate, monitor units, and irradiation time, are presented in Table 2.

The presence of the lung shield resulted in a consistent reduction of the measured dose at all evaluated depths. For a lead-equivalent thickness of 0.8 cm, mean attenuations of 26.60%, 25.89%, and 24.77% were observed at depths of 5 cm, 10 cm, and 15 cm, respectively. These results demonstrate that the device exhibits stable attenuation capability throughout the irradiated volume, with variation below 2% across depths, indicating physically homogeneous behavior of the lead-sphere filling.

Table 2. Conversion of dosimetric readings into absorbed dose (cGy), dose rate (cGy/MU), monitor units, and irradiation time per field.

	Depth 5 cm			Depth 10 cm			Depth 15 cm		
	No shield	**Right**	**Left**	**No shield**	**Right**	**Left**	**No shield**	**Right**	**Left**
Dose (cGy)*	14.366 ± 0.029	10.466 ± 0.010	10.624 ± 0.011	15.215 ± 0.009	11.198 ± 0.011	11.353 ± 0.011	15.894 ± 0.010	11.885 ± 0.012	12.028 ± 0.012
Dose rate (cGy/MU)	0.0718	0.0523	0.0531	0.0761	0.0560	0.0568	0.0795	0.0594	0.0601
MU per field (MU)	1392.14	1911.02	1882.50	1314.52	1786.05	1761.67	1258.32	1682.84	1662.72
Time per field (min)	6.961	9.555	9.412	6.573	8.930	8.808	6.292	8.414	8.314

Source: The author (2025). *Dose corrected for temperature and pressure ($k_{T,P}$), beam quality correction factor (k_{Q,Q_0}), calibration factor (N_{D,w,Q_0}), and percentage depth dose (PDD). Uncertainty values correspond to the propagated experimental standard deviation derived from repeated ionization charge measurements.

Figure 5 shows the comparison between the attenuation rates of the right and left shields and the reference values previously established as desirable for the attenuation function. The comparison between right and left shields reveals similar dosimetric response for both, confirming the reproducibility of the manufacturing process and the uniform distribution of attenuating material within the 3D-printed mold.

The obtained attenuation values are consistent with the literature on lung shielding in TBI. Experimental studies report dose reductions of approximately 25% using similar lead thicknesses, as observed by Nash et al. (14), reinforcing the capability of the developed device to achieve attenuation levels suitable for clinical lung-protection applications. Thus, the results confirm that granular filling with metallic spheres can reproduce the expected attenuation performance of equivalent solid shields.

To evaluate the effectiveness of the shield developed in this study, the percentage deviation (D%) (Equation 5) of the measured lung dose relative to the reference dose of 8 Gy was calculated:

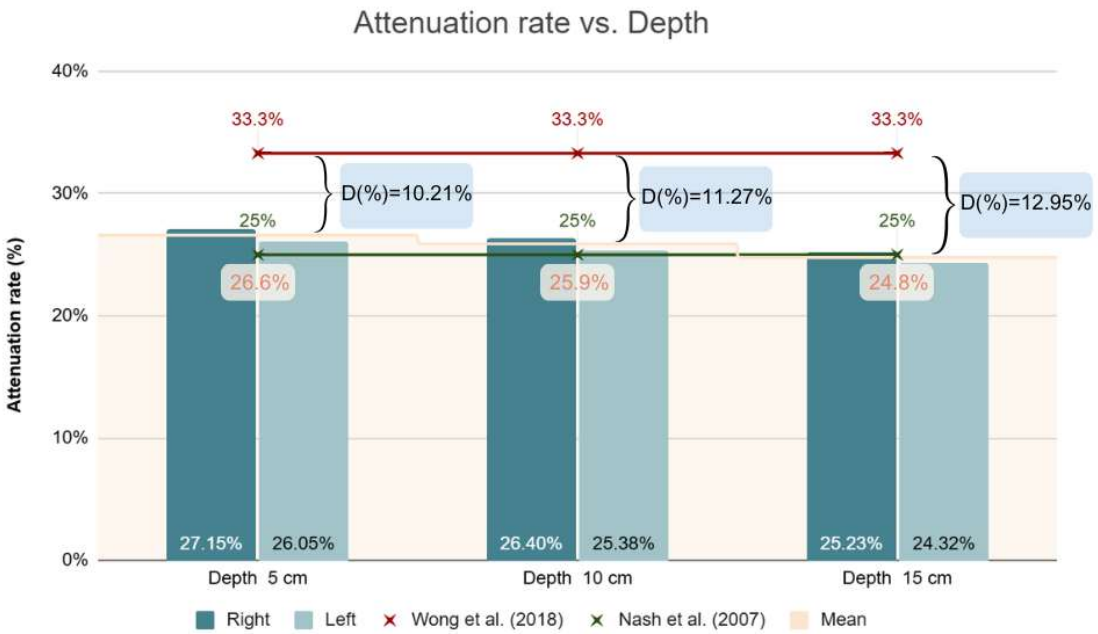

Figure 5. Comparison between attenuation rates of the right and left shields and the desired attenuation values. Source: The author.

$$D(\%) = \left[\left(\frac{dos\ \ wit\ \ shiel\ \ - desired\ dose}{desired\ dose}\right) \times 100\right] \quad (5)$$

Considering that the measurements were performed in a homogeneous water-equivalent phantom, the obtained values do not directly represent lung dose under real clinical conditions, since lung tissue presents low density and structural heterogeneity. In this context, the adopted experimental model was primarily intended to validate the device's dosimetric behavior, particularly its attenuation capability and volumetric uniformity.

The difference between the mean experimental attenuation obtained and the theoretical attenuation estimated for the employed equivalent thickness was 11.48%, indicating adequate agreement between the device performance and the reference value adopted for the attenuating material under homogeneous conditions.

Considering patient body thickness in TBI, the simulated depths correspond to different age groups: 5 cm, 10 cm, and 15 cm approximately correspond to anteroposterior separations (AP) of 10 cm, 20 cm, and 30 cm, respectively, simulating a pediatric, adolescent, and adult patient. In a study by Yaparpalvi et al. (15), phantom measurements showed that a lead thickness of 9 mm is required to obtain 70-75% lung transmission with 15 MV beams in pediatric patients.

The results demonstrate that the device provided consistent attenuation between the right and left sides, indicating homogeneous granular filling and reproducible fabrication. Additive manufacturing enabled anatomically precise geometry with reduced preparation time compared to cast metallic shields. The use of lead spheres in polymer molds eliminates metal-melting steps, reducing occupational risks and manufacturing costs.

4. Conclusion

The present study demonstrated the feasibility of developing patient-specific lung shields via additive manufacturing with granular lead-sphere filling for application in total-body irradiation.

The results confirm the physical attenuation efficiency, the volumetric uniformity of the attenuating material within the printed mold, and the reproducibility between the right and left shields, thereby validating the proposed fabrication method. The low attenuation variation across depths indicates stable dosimetric behavior of the device throughout the irradiated volume.

In addition to its dosimetric performance, the methodology presents relevant practical advantages, including anatomical customization, elimination of metal casting processes, and simplification of clinical preparation. Although the homogeneous phantom used does not reproduce the heterogeneity of human lung tissue, it enables controlled evaluation of the device's attenuation behavior and internal uniformity, being appropriate for the physical validation of the shielding model.

Thus, the developed shield proved to be technically feasible and physically effective as a lung-shielding device; however, further studies in heterogeneous phantoms and clinical settings are required to complement its validation and confirm its applicability under real anatomical conditions.

References

1. Vogel J, Hui S, Hua C-H, Dusenbery K, Rassiah P, Kalapurakal J, et al. Pulmonary Toxicity After Total Body Irradiation – Critical Review of the Literature and Recommendations for Toxicity Reporting. Front. Oncol. 2021;11:708906.
2. Wong JY, Filippi AR, Dabaja BS, Yahalom J, Specht L. Total body irradiation: guidelines from the international lymphoma radiation oncology group (ILROG). International Journal of Radiation Oncology* Biology* Physics. 2018;101(3):521-529.
3. Furnari L. Controle De Qualidade Em Radioterapia. Revista Brasileira de Física Médica. 2015;3:77-90.

4. Salvajoli JV, Souhami L, Faria SL. Radioterapia em Oncologia. 2nd ed. São Paulo: Atheneu; 2023.
5. Brasil. Ministério da Saúde. Instituto Nacional de Câncer. Curso para técnicos em radioterapia. Rio de Janeiro: INCA; 2000.
6. IARC Working Group on the Evaluation of Carcinogenic Risks to Humans. Arsenic, Metals, Fibres and Dusts. Lyon (FR): International Agency for Research on Cancer; 2012. (IARC Monographs on the Evaluation of Carcinogenic Risks to Humans, No. 100C.) CADMIUM AND CADMIUM COMPOUNDS.
7. Silva HR, Rebello WF, Silva AX, Facure A. Development of a shielding to protect patients against photoneutrons produced by linacs in radiotherapy treatments. Revista Brasileira de Física Médica. 2011;5(2):201-204.
8. Mankovich NJ, Baik H, Baumgartner HA, Hiller JB. Synthetic tomographic image phantom for 3D validation. In Medical Imaging 1993: Image Capture, Formatting, and Display. SPIE. 1993;1897:170-176.
9. Poulin E, Gardi L, Fenster A, Pouliot J, Beaulieu L. Towards real-time 3D ultrasound planning and personalized 3D printing for breast HDR brachytherapy treatment. Radiotherapy and Oncology. 2015;114(3):335-338.
10. Vianna ERL, Schwarz AP. Desenvolvimento e Construção de um Fantoma de Tórax para Uso nos Estudos de Imagens Radiológicas. Trabalho Final de Graduação - Universidade Franciscana; 2020.
11. Nist.gov. [homepage on the Internet]. National Institute of Standards and Technology. X-Ray Mass Attenuation Coefficients – Chapter 2: Introduction to Tables and Graphs. [cited 2025 Mar 23]. Available from: https://physics.nist.gov/PhysRefData/XrayMassCoef/chap2.html.
12. Nist.gov. [homepage on the Internet]. National Institute of Standards and Technology. X-Ray Mass Attenuation Coefficients – Lead (z = 82). [cited 2025 Mar 23]. Available from: https://physics.nist.gov/PhysRefData/XrayMassCoef/ElemTab/z82.html.
13. Van Dyk J, Galvin JM, Glasgow GP, Podgorsak EB. The physical aspects of total and half body photon irradiation. AAPM report. 1986;17:22-24.
14. Nash RA, McSweeney PA, Crofford LJ, Abidi M, Chen CS, Godwin JD, et al. High-dose immunosuppressive therapy and autologous hematopoietic cell transplantation for severe systemic sclerosis: long-term follow-up of the US multicenter pilot study. Blood, The Journal of the American Society of Hematology. 2007;110(4):1388-1396.
15. Yaparpalvi R, Mynampati DK, Fox JL, Tome WA, Kalnicki S. A Simple Technique for Partial Transmission Lung Shielding in Pediatric Patients Undergoing TBI for HSCT. International Journal of Radiation Oncology, Biology, Physics. 2019;105(1):E715.

Contact:

Luísa Vargas Cassol
Universidade Franciscana - UFN
R. dos Andradas, 1614 - Centro, Santa Maria - RS, 97010-030
luisacassol@gmail.com

APPENDIX I

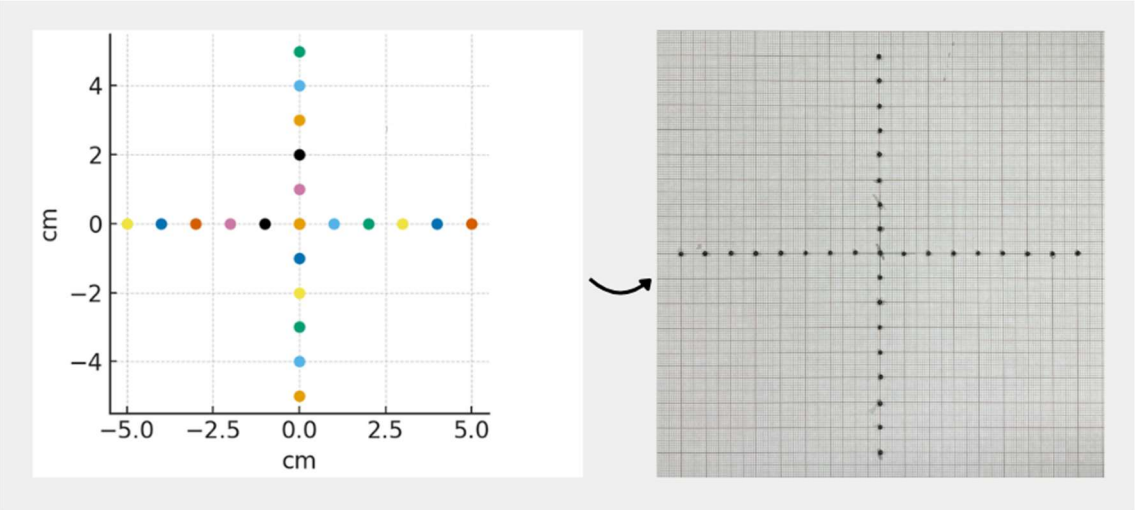

Supplementary Figure S1. Cross-shaped arrangement of spheres with 1.0 cm spacing used for magnification factor estimation.